BIOCHEMISTRY
including biophysical chemistry & molecular biology
Article

Biochemistry **2010,** *49,* 7227–7237 7227
DOI: 10.1021/bi100805b

Structural Analysis of WbpE from *Pseudomonas aeruginosa* PAO1: A Nucleotide Sugar Aminotransferase Involved in O-Antigen Assembly[†,‡]

Angelyn Larkin,[∥] Nelson B. Olivier,[∥] and Barbara Imperiali*[,∥,§]

[∥]*Department of Chemistry and* [§]*Department of Biology, Massachusetts Institute of Technology, 77 Massachusetts Avenue, Cambridge, Massachusetts 02139*

Received May 20, 2010; Revised Manuscript Received July 3, 2010

ABSTRACT: In recent years, the opportunistic pathogen *Pseudomonas aeruginosa* has emerged as a major source of hospital-acquired infections. Effective treatment has proven increasingly difficult due to the spread of multidrug resistant strains and thus requires a deeper understanding of the biochemical mechanisms of pathogenicity. The central carbohydrate of the *P. aeruginosa* PAO1 (O5) B-band O-antigen, ManNAc-(3NAc)A, has been shown to be critical for virulence and is produced in a stepwise manner by five enzymes in the Wbp pathway (WbpA, WbpB, WbpE, WbpD, and WbpI). Herein, we present the crystal structure of the aminotransferase WbpE from *P. aeruginosa* PAO1 in complex with the cofactor pyridoxal 5′-phosphate (PLP) and product UDP-GlcNAc(3NH$_2$)A as the external aldimine at 1.9 Å resolution. We also report the structures of WbpE in complex with PMP alone as well as the PLP internal aldimine and show that the dimeric structure of WbpE observed in the crystal structure is confirmed by analytical ultracentrifugation. Analysis of these structures reveals that the active site of the enzyme is composed of residues from both subunits. In particular, we show that a key residue (Arg229), which has previously been implicated in direct interactions with the α-carboxylate moiety of α-ketoglutarate, is also uniquely positioned to bestow specificity for the 6″-carboxyl group of GlcNAc(3NH$_2$)A through a salt bridge. This finding is intriguing because while an analogous basic residue is present in WbpE homologues that do not process 6″-carboxyl-modified saccharides, recent structural studies reveal that this side chain is retracted to accommodate a neutral C6″ atom. This work represents the first structural analysis of a nucleotide sugar aminotransferase with a bound product modified at the C2″, C3″, and C6″ positions and provides insight into a novel target for treatment of *P. aeruginosa* infection.

Pseudomonas aeruginosa is a Gram-negative pathogen responsible for severe infection in immunocompromised individuals. In recent years, it has emerged as a major source of hospital-acquired infections, such as bacteremia, pneumonia, and febrile neutropenia, and leads to inflammation and pulmonary failure in cystic fibrosis patients (*1*−*5*). While there are several standard antibiotics currently used to combat *P. aeruginosa*, the rapidly increasing occurrence of multidrug resistant strains has complicated treatment and highlighted the need for alternative drug design strategies (*6*−*8*). One of the most promising targets for improved treatment is the bacterial lipopolysaccharide (LPS),[1] found in the exterior leaflet of the outer membrane of the organism. The LPS of *P. aeruginosa* contains the B-band O-antigen unit, a critical virulence factor that has been shown to play a key role in host colonization and evasion of immune defenses (*9*−*11*). Genetic mutants of *P. aeruginosa* deficient in B-band O-antigen have exhibited greatly increased sensitivity to phagocytosis and serum-mediated killing (*12*).

The B-band O-antigen of *P. aeruginosa* PAO1 (serotype O5) is composed of repeating units of a trisaccharide made up of 2-acetamido-3-acetamidino-2,3-dideoxy-β-D-mannuronic acid (ManNAc(3NAm)A), 2,3-diacetamido-2,3-dideoxy-β-D-mannuronic acid (ManNAc(3NAc)A), and *N*-acetyl-α-D-fucosamine (Fuc2NAc) (*13*). Recent studies have shown that the central saccharide unit, ManNAc(3NAc)A, is synthesized by five enzymes in the Wbp pathway (WbpA, WbpB, WbpE, WbpD, and WbpI) starting from the common precursor, UDP-GlcNAc (Figure 1) (*14*). In the first step, WbpA oxidizes the C6″ hydroxyl group to afford UDP-GlcNAcA. This is followed by the coupled action of the dehydrogenase WbpB and aminotransferase WbpE to yield UDP-GlcNAc(3NH$_2$)A through a unique NAD$^+$ recycling pathway (*15*). Finally, the acetyltransferase WbpD and epimerase WbpI provide the final UDP-ManNAc(3NAc)A donor, which is then transferred to an undecaprenyl carrier. After completion, the trisaccharide is flipped into the bacterial periplasm by the Wzx translocase and then ligated to the growing O-antigen by Wzy polymerase (*16*).

[†]This work was supported by National Institutes of Health Grant GM039334 to B.I.

[‡]X-ray coordinates (accession codes 3NU7, 3NU8, and 3NUB) have been deposited in the Protein Data Bank, Research Collaboratory for Structural Bioinformatics, Rutgers University, New Brunswick, NJ.

*To whom correspondence should be addressed: Massachusetts Institute of Technology, 77 Massachusetts Ave., Cambridge, MA 02139. Phone: (617) 253-1838. Fax: (617) 452-2419. E-mail: imper@mit.edu.

[1]Abbreviations: AAT, aspartate aminotransferase; Bis-Tris, 2-bis(2-hydroxyethyl)amino-2-(hydroxymethyl)-1,3-propanediol; CE, capillary electrophoresis; DTT, dithiothreitol; EDTA, ethylenediaminetetraacetic acid; HEPES, 4-(2-hydroxyethyl)-1-piperazineethanesulfonic acid; IPTG, isopropyl β-D-1-thiogalactopyranoside; α-KG, α-ketoglutarate; LPS, lipopolysaccharide; Ni-NTA, nickel nitrilotriacetic acid; PLP, pyridoxal 5′-phosphate; PMP, pyridoxamine 5′-phosphate; rmsd, root-mean-square deviation; RP-HPLC, reverse-phase high-performance liquid chromatography; TEAB, triethylammonium bicarbonate; TEV, tobacco etch virus; UDP, uridine 5′-diphosphate; UDP-GlcNAc, UDP-*N*-acetyl-D-glucosamine; UDP-GlcNAcA, UDP-*N*-acetyl-D-glucosaminuronic acid; UDP-GlcNAc(3keto)A, UDP-2-acetamido-2-deoxy-3-oxo-D-glucuronic acid; UDP-GlcNAc(3NH$_2$)A, UDP-2-acetamido-3-amino-2,3-dideoxy-D-glucuronic acid; UDP-ManNAc(3NAc)A, UDP-2,3-diacetamido-2,3-dideoxy-D-mannuronic acid.

Published on Web 07/06/2010

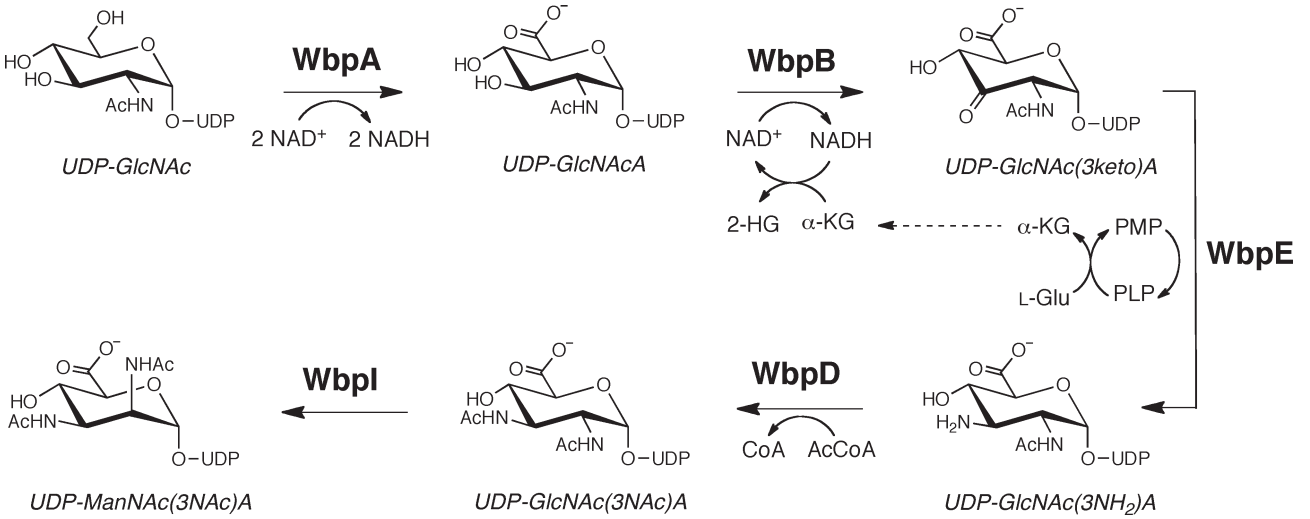

FIGURE 1: Biosynthetic pathway of UDP-ManNAc(3NAc)A in *P. aeruginosa* PAO1 (serotype O5). Abbreviations: AcCoA, acetyl-coenzyme A; CoA, coenzyme A; 2-HG, 2-hydroxyglutarate; α-KG, α-ketoglutarate; NAD^+, nicotinamide adenine dinucleotide; NADH, nicotinamide adenine dinucleotide (reduced); PLP, pyridoxal 5′-phosphate; PMP, pyridoxamine 5′-phosphate.

WbpE is a pyridoxal 5′-phosphate (PLP)-dependent aminotransferase responsible for the conversion of UDP-GlcNAc(3keto)A and L-glutamate to UDP-GlcNAc($3NH_2$)A and α-ketoglutarate (α-KG), respectively. It is a member of the broad class of Fold Type I aspartate-aminotransferase (AAT) enzymes, which harness the powerful electron-sink properties of PLP to conduct a wide variety of transformations, including transaminations, eliminations, decarboxylations, and racemizations (*17*, *18*). The general mechanism of this class of enzymes has been studied in great detail and is divided into two discrete half-reactions that cycle between the PMP and PLP forms of the cofactor (Figure 2). The reaction begins with formation of an imine between the ketone-bearing sugar and PMP, followed by abstraction of a C4′ proton of PMP by the catalytic lysine residue of the protein. The resulting quinoid intermediate then accepts a proton from the lysine at the C3″ carbon of the pyranose, which serves to set the stereochemistry at this position and results in the external aldimine intermediate. Release of the nucleotide sugar amine product is facilitated by transimination to afford the internal aldimine. In the second half of the catalytic cycle, the reaction steps are repeated in the reverse order, resulting in regeneration of PMP through conversion of L-glutamate to α-ketoglutarate.

In this report, we present the crystal structure of the aminotransferase WbpE from *P. aeruginosa* PAO1 in complex with three different ligands: PMP, PLP, and the external aldimine of PLP with the reaction product UDP-GlcNAc($3NH_2$)A. In recent years, the crystal structures of several Fold Type I enzymes that catalyze the transamination of nucleotide sugars in bacteria have been described (*19*−*24*). These studies have revealed that while members of this enzyme class share many similarities in the cofactor-binding site, the factors that govern the binding and specificity of the nucleotide sugar substrates are not yet fully understood. This work presents the first structure of an aminotransferase that binds a nucleotide sugar modified at the C2″, C3″, and C6″ positions and thus provides a glimpse into the means by which a highly functionalized nucleotide sugar is accommodated in the enzyme active site. In addition, we confirm that WbpE associates as a homodimer in solution using sedimentation velocity analytical ultracentrifugation. To gain a broader understanding of nucleotide sugar specificity across this class of aminotransferases, we compare our WbpE structure in complex with the external aldimine to the other nucleotide sugar-bound aminotransferase structures. We envision that this work will add to the growing body of knowledge about nucleotide sugar aminotransferases and may also present a novel target for the development of antimicrobial treatments to combat *P. aeruginosa*.

EXPERIMENTAL PROCEDURES

Molecular Biology. The *wbpE* gene was amplified from *P. aeruginosa* PAO1-LAC genomic DNA (ATCC) by the polymerase chain reaction as previously described, using primers to introduce 5′ *Bam*HI and 3′ *Xho*I restriction sites (*15*). The resulting oligonucleotide was then inserted into a modified pET32a vector (Novagen) using standard molecular biology techniques. Site-directed mutagenesis was performed using the QuikChange protocol from Stratagene with the *wbpE*-pET32a plasmid as a template. All constructs yielded proteins with an N-terminal His_6 tag followed by a tobacco etch virus (TEV) protease site for tag removal.

Overexpression of WbpE. The *wbpE*-pET32a plasmid was transformed into *E. coli* BL21-CodonPlus(DE3) RIL competent cells (Stratagene) for heterologous expression, using both kanamycin (50 μg/mL) and chloramphenicol (30 μg/mL) for selection. The cell culture was grown to an optical density (600 nm) of 0.8−1.0 at 37 °C in Luria-Bertani broth; the culture was subsequently cooled to 16 °C, and protein expression was induced through the addition of IPTG (1 mM). After 16 h, the cells were harvested by centrifugation (5000*g*), and the resulting cell pellets were stored at −80 °C for future use. Incorporation of selenomethionine was accomplished using the method of metabolic inhibition described elsewhere with slight modification (*25*). Briefly, 0.5 L of M9 medium supplemented with 1 mM $MgSO_4$, 3 mM $FeSO_4$, 0.4% (w/v) glucose, 0.5% (w/v) thiamine, kanamycin (50 μg/mL), and chloramphenicol (30 μg/mL) was inoculated with a 5 mL starter culture and allowed to incubate at 37 °C until the desired optical density (0.8−1.0) was obtained. Prior to induction, the following amino acids were added to the flask and the culture was incubated for 15 min to allow the inhibition of methionine biosynthesis: L-lysine (100 mg/L), L-phenylalanine (100 mg/L), L-threonine (100 mg/L), L-isoleucine (50 mg/L),

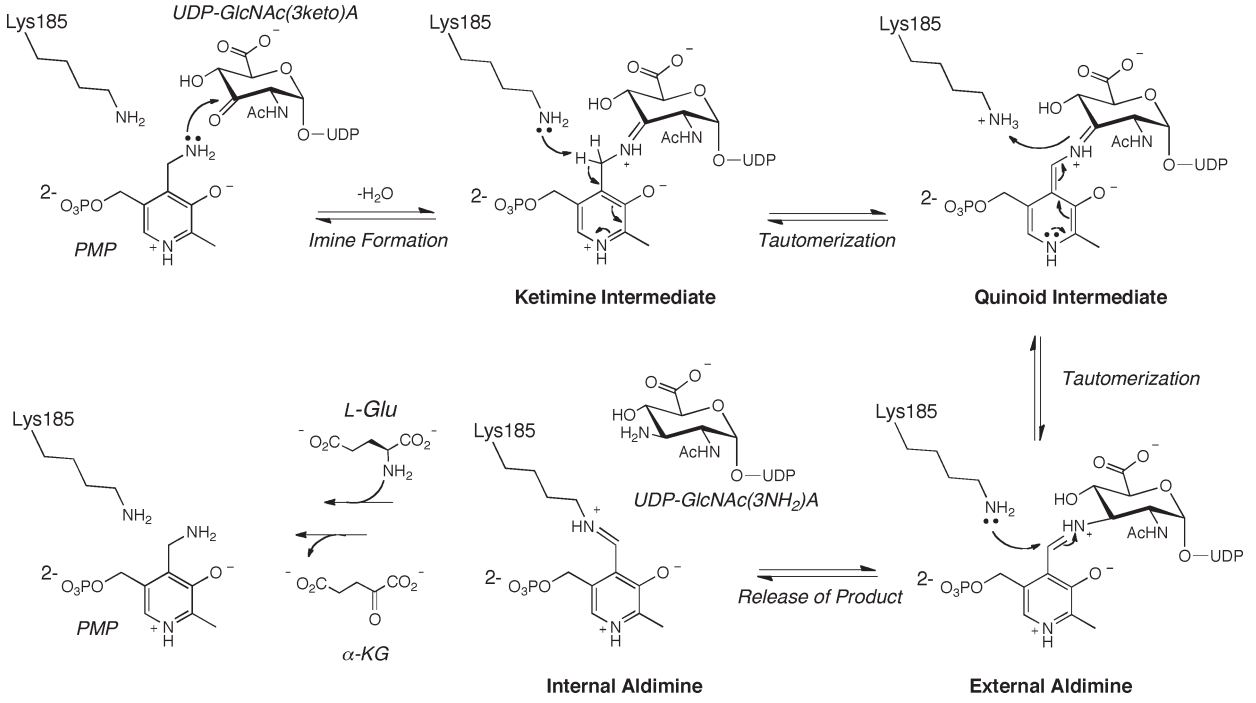

FIGURE 2: Proposed reaction mechanism of WbpE.

L-leucine (50 mg/L), L-valine (50 mg/L), and L-selenomethionine (60 mg/L). After addition of IPTG (1 mM) to induce protein expression, the culture was handled as described above.

Purification of WbpE. All steps were performed at 4 °C. WbpE was purified from cell pellets using Ni-NTA resin (Qiagen) as previously described (*15*). After overnight dialysis to remove the imidazole and lower the salt concentration, the N-terminal His_6 tag was removed by incubation with TEV protease over the course of 3 days while the mixture was being stirred in dialysis buffer [50 mM HEPES (pH 8.0), 100 mM NaCl, 4% glycerol, 0.5 mM EDTA, and 5 mM DTT]; the removal of the tag was confirmed by Western blot analysis using an Anti-His_4 anitbody (Qiagen). The protein was then subjected to size-exclusion chromatography using a Superdex 200 16/60 column (GE Healthcare) in running buffer composed of 25 mM HEPES (pH 8.0), 100 mM NaCl, and 0.5% glycerol. Fractions containing monodispersed protein were pooled and analyzed by SDS−PAGE for purity and MALDI mass spectrometry to quantify selenomethionine incorporation. Purified protein was routinely utilized within 24 h to prevent aggregation.

Sedimentation Velocity Analytical Ultracentrifugation. Experiments were conducted in an Optima XL-I ultracentrifuge (Beckman Coulter) using an An60 Ti rotor at 4 °C with a rotor speed of 42000 rpm. Data were acquired by monitoring the absorbance at 280 nm through quartz cell windows. A sample of WbpE (36 μM) was dialyzed against 25 mM HEPES (pH 8.0), 100 mM NaCl, and 0.5% glycerol for 24 h prior to the experiment; the centrifugation run also included dialysis buffer as a blank. Data were analyzed with the software package SEDANAL (*26*) to determine the oligomeric state of the protein in solution.

Synthesis of UDP-GlcNAc($3NH_2$)A. The UDP-GlcNAc-($3NH_2$)A product of WbpE was prepared starting from UDP-GlcNAcA using the coupled enzyme reaction of WbpB and WbpE as previously described with slight modification (*15*). UDP-GlcNAcA (0.75 mM), NAD^+ (0.2 mM), L-glutamate (25 mM), PLP (0.1 mM), DTT (2.5 mM), and $MgCl_2$ (2 mM) were combined in 50 mL of HEPES buffer (50 mM, pH 8.0) with 4.5 mg each of WbpB and WbpE and incubated for 10 h at 30 °C. After filtration to remove protein, the crude reaction mixture was purified using a Synergi C_{18} Hydro preparatory RP-HPLC column (4 μm, 80 Å, 250 mm × 21.2 mm, Phenomenex) equilibrated with 50 mM TEAB (pH 7.1); the desired product was eluted with a linear gradient from 0 to 50% CH_3CN over 85 min. To remove the TEAB salt for crystallization, UDP-GlcNAc($3NH_2$)A was dissolved in distilled, deionized water and subjected to cation exchange chromatography using a 1 mL HiTrap SP FF column (GE Healthcare).

Crystallization and Data Collection. Prior to the setup of crystal trays, WbpE was concentrated to 10 mg/mL in the size-exclusion running buffer. For crystallization in the presence of ligands, PLP, UDP-GlcNAc($3NH_2$)A, or both were added to the protein solution at final concentrations of 50 μM and 10 mM, respectively, and allowed to incubate on ice for 1 h. Crystals were obtained at 25 °C from a hanging drop by mixing 1.5 μL of protein solution with 1.5 μL of reservoir solution. All crystals except for the SeMet derivative were grown in a reservoir solution containing 0.1 M Bis-Tris (pH 5.5), 0.2 M ammonium sulfate, and 25% PEG 3350. SeMet crystals were grown in a reservoir solution containing 0.1 M Bis-Tris (pH 5.5), 0.2 M ammonium acetate, 10 mM $SrCl_2$, and 25% PEG 3350. Crystals were cryoprotected in the corresponding reservoir solution supplemented with 20% glycerol and substrate as necessary. Diffraction data were collected on beamline X6A (National Synchrotron Light Source, Brookhaven National Laboratory, Upton, NY) at 110 K. For the SeMet derivative, data were collected at the selenium peak (12667 eV), edge (12660 eV), and remote (12867 eV). Data sets were indexed and scaled using HKL2000 (*27*), and the scaled intensities were converted to structure factors using the program TRUNCATE in the CCP4 suite of programs (*28*). Data collection parameters are listed in Table 1.

Structure Determination and Refinement. The structure of the WbpE−SeMet derivative was determined using the method of multiwavelength anomalous diffraction (*29*). Using data

Table 1: Data Collection and Refinement Statistics

	PMP	PLP	external aldimine	SeMet[a]
Data Collection				
space group	$P2_12_12$	$P2_12_12$	$P2_12_12$	$P2_12_12$
unit cell dimensions (*a*, *b*, *c*) (Å)	78.28, 149.29, 54.90	77.79, 148.72, 53.22	78.29, 149.67, 55.12	77.81, 149.03, 53.29
resolution (Å)	50.0−1.95	20.0−1.50	20.0−1.83	50.0−1.93
no. of observed reflections	45308	94182	46379	46078
R_{merge} (%)[b,c]	7.3 (42.0)	9.1 (66.2)	7.1 (49.2)	8.2 (41.9)
$I/\sigma I$[b,c]	53.4 (9.2)	35.8 (3.0)	36.3 (4.1)	36.7 (5.8)
completeness (%)[c]	99.8	99.7	98.6	100
redundancy[b,c]	14.6 (14.5)	7.9 (7.0)	7.3 (6.7)	7.5 (7.2)
Refinement				
resolution (Å)	35−1.95	20−1.50	20−1.90	
R_{work}/R_{free} (%)[d]	19.8/24.6	19.7/22.2	19.9/24.5	
total no. of atoms	5837	5880	6027	
protein	5428	5471	5401	
water	377	409	516	
ligands	32	32	110	
B factor (Å^2)				
overall	28.2	20.5	19.8	
protein	28.3	19.1	19.3	
water	29.4	22.7	27.4	
ligand	15.0	16.9	34.8	
Ramachandram plot (%)[e]	96.8/2.8/0.4	97.1/2.7/0.3	96.0/3.8/0.3	
rmsd				
bond lengths (Å)	0.010	0.007	0.010	
bond angles (deg)	1.245	1.152	1.204	
PDB entry	3NU7	3NU8	3NUB	

[a]Data reported for the SeMet derivative refer to those collected at the selenium peak wavelength. [b]The numbers in parentheses represent data for the highest-resolution bin: 1.98−1.94, 1.55−1.5, 1.86−1.83, and 2.01−1.93 Å for the data sets of PMP, PLP, external aldimine, and the SeMet derivative, respectively. [c]$R_{merge} = \sum|I - \langle I\rangle|/\sum I$, where I is the intensity of a reflection and $\langle I\rangle$ is the mean intensity of a group of equivalent reflections. [d]$R_{work} = \sum_h||F(h)_{obs}| - |F(h)_{calc}||/\sum_h|F(h)_{obs}|$. R_{free} was calculated for 5% of the reflections randomly excluded from the refinement. [e]Ramachandran plot statistics are given as core/allowed/generously allowed and are for both chains.

collected at the selenium peak and truncated to 2.5 Å, SOLVE (*30*) was employed to locate the heavy atom sites and generate experimental phases. A total of four of five selenium atoms were located for each protein subunit. The initial model was built using the prime-and-switch phasing feature of RESOLVE (*31*, *32*) to minimize model bias and contained the basic framework of the model, except for sizable gaps between residues 116−142 and 196−233. The PMP-bound structure was then determined by molecular replacement using Phaser (*33*) with the SeMet derivative as the initial search model. Further model building and refinement were conducted using Coot (*34*) and Refmac (*35*). Five percent of the data was used to calculate the R_{free} values for cross-validation of the refinement process (*36*). The structures of the PLP and external aldimine complexes were subsequently determined by molecular replacement in the same manner, using the completed PMP-bound structure with the cofactor removed as the input model. Water molecules were added using both ARP/wARP (*37*) and Coot, and ligands were modeled into each structure after the R_{free} value was $<30\%$. All refined structures were validated using PROCHECK (*38*), SFCHECK (*39*), and MolProbity (*40*), and the final refinement statistics are listed in Table 1. All molecular images were generated using PyMOL.

Functional Characterization of WbpE Alanine Mutants. Enzyme mutants were analyzed for function using the coupled WbpB/WbpE assay slightly modified from that described previously (*15*). In brief, 2.5 μg of each WbpE mutant was incubated with UDP-GlcNAcA (0.75 mM), NAD^+ (0.2 mM), L-glutamate (25 mM), PLP (0.1 mM), DTT (2.5 mM), $MgCl_2$ (2 mM), and 2.5 μg of WbpB in 60 μL of 50 mM HEPES buffer (pH 8.0) for 2 h at 30 °C. Capillary electrophoresis (P/ACE MDQ System, Beckman Coulter) was used to monitor enzyme activity as outlined previously, and the presence of product was confirmed by the addition of starting material to the reaction mixtures and the observation of a new peak on the CE chromatogram.

RESULTS

Overall Architecture of WbpE. WbpE crystallized in orthorhombic space group $P2_12_12$, with two molecules in the asymmetric unit and the following approximate unit cell dimensions: 75 Å × 150 Å × 50 Å (Figure 3). The overall scaffold of WbpE is similar to that of other members in the Fold Type 1 aminotransferase family, with aspartate aminotransferase (AAT) representing the first and most well-studied member (*41*, *42*). As in the case of AAT, each monomer of WbpE can be divided into two major domains: a large N-terminal PLP-binding region and a smaller C-terminal domain (Figure 3C). The N-terminal portion (residues Ile14−Glu243) is composed of a total of 11 β-strands, seven of which make up a central β-sheet that exhibits the following canonical strand order: β-1, β-9, β-8, β-5, β-4, β-2, β-3, where β-9 is antiparallel to the others. This β-sheet is bordered on the top and bottom faces by seven α-helices. After strand β-9, a short stretch of residues (Gln209−Arg229) extends out from the monomer structure to form a large domain-swapped β-hairpin (β-10 and β-11) that interacts with the active site of the other monomer. Another smaller β-hairpin (residues Ala163−Ser170, β-6, and β-7) protrudes from the top face of the central β-sheet and interacts with the C-terminal region in the same

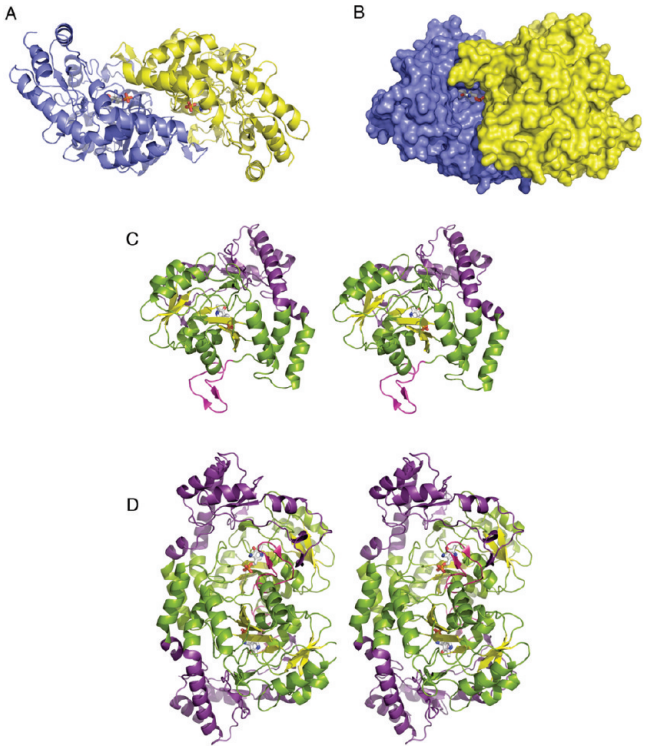

FIGURE 3: Crystal structure of the WbpE−PMP complex. (A) Structure of the homodimer, with each subunit colored individually and the PMP cofactor shown as sticks. (B) Space-filling model of the homodimer, where the PMP cofactor can be observed at the end of the deep cavity. (C) Stereodiagram of a single subunit, with the N- and C-terminal domains colored green and purple, respectively. The β-strands comprising the central β-sheet are highlighted in yellow, and the domain-swapped β-hairpin is colored magenta. (D) Stereodiagram of the homodimer, with the various domain features colored as described for panel C.

subunit. The C-terminal portion of the protein (residues Met1−Arg13 and Ile244−Asn359) consists of two short β-strands and six α-helices that are oriented away from each other in a V shape. The entire C-terminal region of the protein is closely aligned with the N-terminal domain on the top face of the monomer yet opens to reveal a deep channel on the opposite face of the subunit, allowing solvent access to the enzyme active site (Figure 3B). In addition, this domain of the protein contains a non-prolyl *cis* amide bond between residues His308 and Tyr309.

The interface between the subunits of the dimer is extensive and comprises an area of approximately 7500 Å^2, which represents nearly 25% of the total surface area of a single subunit. The two active sites of the dimer are open to one another and are spaced ~30 Å apart. The most striking interaction between the two monomers is the presence of the domain-swapped β-hairpin that crosses over the dimer interface and lines the entrance to the active site tunnel of the neighboring subunit. Other notable interactions between the monomers include the stacking of two homologous antiparallel α-helices from each monomer, both comprising residues Ile14−His28, as well as the loop residues Cys189−Gly193 from one subunit that nestle beneath residues Gly29−Leu33 from the other (Figure 3).

Sedimentation velocity analytical ultracentrifugation studies were undertaken to establish whether the dimerization of WbpE observed in the crystal structure correlates with the oligomeric state present in solution. The sedimentation coefficient was found to be 4.72 Sv, and the molecular mass was calculated as 79.3 kDa using a single-species model fit. As each monomer of WbpE has a theoretical molecular mass of 38.9 kDa, the data suggest that WbpE associates as a dimer in solution (Figure S1 of the Supporting Information). This finding is in keeping with other members of the Fold Type I aminotransferase family, which have been found to exist primarily as homodimers or other higher-order oligomers in mutiples of two (*18*).

Cofactor-Binding Site. During structure refinement, both the SeMet derivative and the native form of WbpE were shown to contain the cofactor bound to the enzyme active site despite the fact that it was not exogenously introduced over the course of protein expression or purification. The electron density of the cofactor was unambiguous and thus modeled into the native structure at full occupancy (Figure 4). It was determined that the cofactor was present in the PMP form due to the retracted position of the catalytic lysine residue (Lys185) as well as the lack of electron density between the C4′ carbon of the cofactor and the lysine nitrogen atom, indicating that there was no covalent bond present. In addition, the UV spectrum of purified WbpE possessed the spectral characteristics of PMP, namely, the presence of an absorbance maximum at 340 nm compared with that at 420 nm indicative of PLP (data not shown). To obtain the PLP-bound form of the enzyme (internal aldimine), PLP was incubated with WbpE for 1 h prior to the setup of crystal trays. In contrast to the PMP-bound crystals, the PLP-bound structure showed an extended conformation of Lys185 and clear electron density between the side chain and the cofactor, serving as evidence that the cofactor was held in place by a covalent bond (Figure 4).

The cofactor-binding site resides within a deep cleft in the interior of each monomer at the far end of the joined active sites. The cofactor is oriented such that the pyridinium ring is facing inward, resting above the central β-sheet of each monomer unit, while the phosphate moiety points toward the entrance of the cleft and is located 20 Å from the phosphate group in the other subunit. The pyridinium ring is flanked on the top face by Tyr85, with which it is interacting in a $\pi-\pi$ stacking fashion, and the bottom face by Ala158. The C5′ hydroxyl group of the cofactor is within hydrogen bonding distance of Gln159 and Tyr309, while the C6′ methyl group is close (3.3 Å) to Val130. The N1 nitrogen atom of the pyridinium ring is held in place by a salt bridge with the carboxylate of Asp156 that serves to enhance the electron-sink properties of the cofactor. This aspartate residue is conserved in all Fold Type I aminotransferases and is crucial for maintaining the cofactor in its protonated state (*17*). In the PMP-bound form of the enzyme, the C4′ amine does not appear to interact with any specific residues, as the closest atom is the oxygen of a water molecule more than 4 Å away. Examination of a space-filling model of the PMP-bound form of WbpE shows that the C4′ amine lies at the bottom of the deep solvent tunnel leading to the outside of the active site, making it accessible for reaction with incoming substrate (Figure 3B). The phosphate group of the cofactor protrudes into the entrance of the active site in the opposite direction and is held in place by several hydrogen bonding and charge stabilizing interactions, including those with Ser180, Thr60, Gly59, and Asn227 of the β-hairpin from the other subunit and three well-ordered water molecules.

An analysis of the residues surrounding the cofactor in both the PMP and PLP-bound structures indicates that there is very little conformational change in the overall architecture of WbpE upon formation of the internal aldimine (Figure 4); the root-mean-square deviation of these two structures is 0.32 Å. Differences include the slight upward shift of the pyridinium ring into

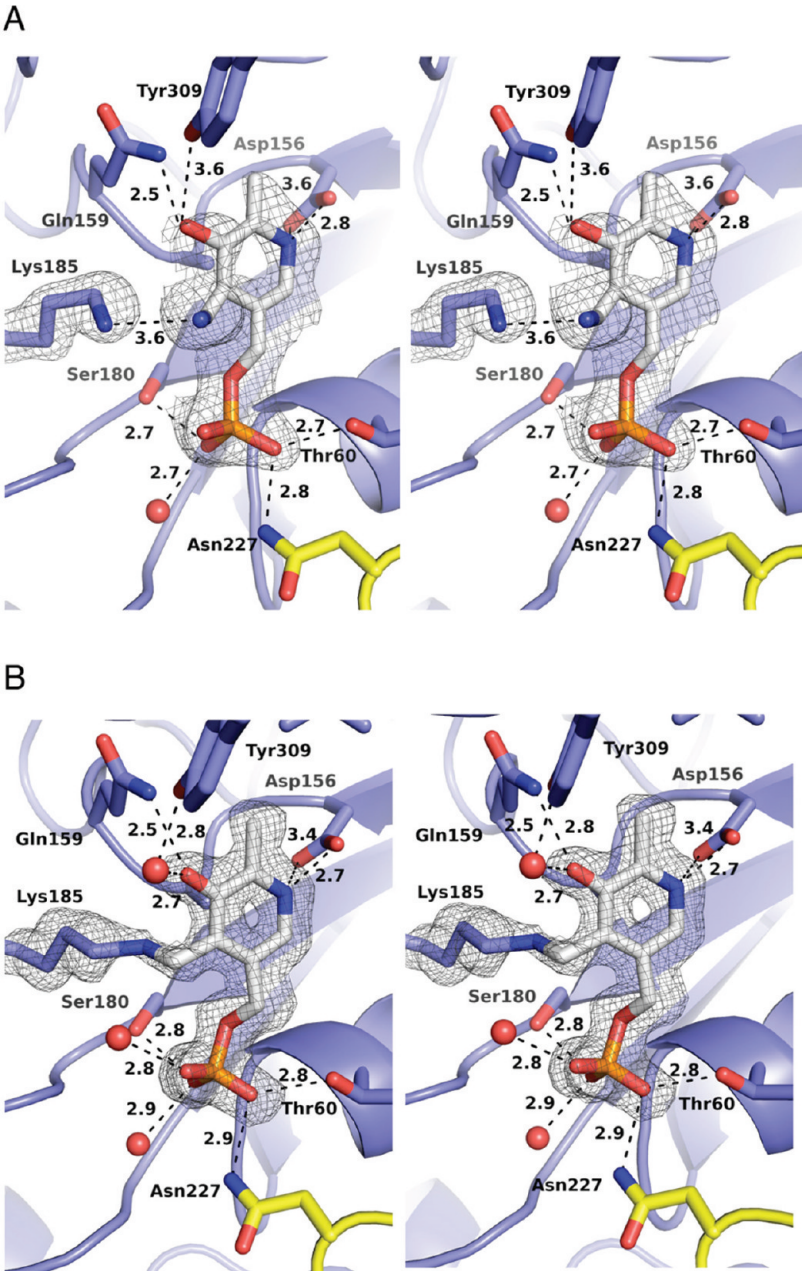

FIGURE 4: Close-up view of the cofactor-binding site. The $2(F_o - F_c)$ electron density maps are contoured at 3σ for both the PMP-bound (A) and PLP-bound (B) structures and were calculated with atoms of the cofactor and Lys185 side chain omitted. Amino acids corresponding to subunits 1 and 2 are colored blue and yellow, respectively, and water molecules are depicted as red spheres. All interactions within 3.6 Å of the cofactor are indicated by dashed lines except for those that line the top face of the cofactor-binding site; these residues were removed from the figure for the sake of clarity but are outlined in the text.

the active site due to the presence of the imine bond as well as small changes in the orientation of the Tyr85 side chain. In addition, the domain-swapped β-hairpin stretches closer toward the active site in the PLP-bound structure; slight changes can be seen in the side chain orientations of Gln215 and Arg212 that reflect this movement.

The Nucleotide Sugar-Binding Site. Crystals of WbpE complexed with the external aldimine were obtained by incubating the enzyme with both PLP and the UDP-GlcNAc(3NH_2)A product on ice for 1 h prior to crystallization. The presence of the external aldimine in the enzyme active site implies that the reaction proceeded in reverse upon exposure to the aminated product; this intermediate was previously observed in other nucleotide sugar-bound aminotransferase structures as well (*20*, *22*, *24*). The external aldimine is bound in both subunits of the dimer, and electron density between the pyridinium C4′ carbon and the C3″ position of the hexose ring indicates the existence of a covalent bond (Figure 5A). As in the case of the WbpE complexes with PMP and PLP, the electron density for the cofactor portion of the ligand is very strong; however, the density for the nucleotide sugar component is weaker, with an average temperature factor $\langle B \rangle$ of 42.8 $Å^2$ compared with that for the cofactor (26.8 $Å^2$) and nearby protein atoms (21.6 $Å^2$). The weakest regions of electron density in the external aldimine structure are surrounding the C4″ hexose carbon as well as the C2′ and C3′ bond in the ribose moiety. This observation suggests that the nucleotide sugar region of the aldimine is not as firmly held in place as the cofactor and may experience some thermal motion within the crystal. For this reason, atoms comprising the nucleotide sugar were refined at 50% occupancy.

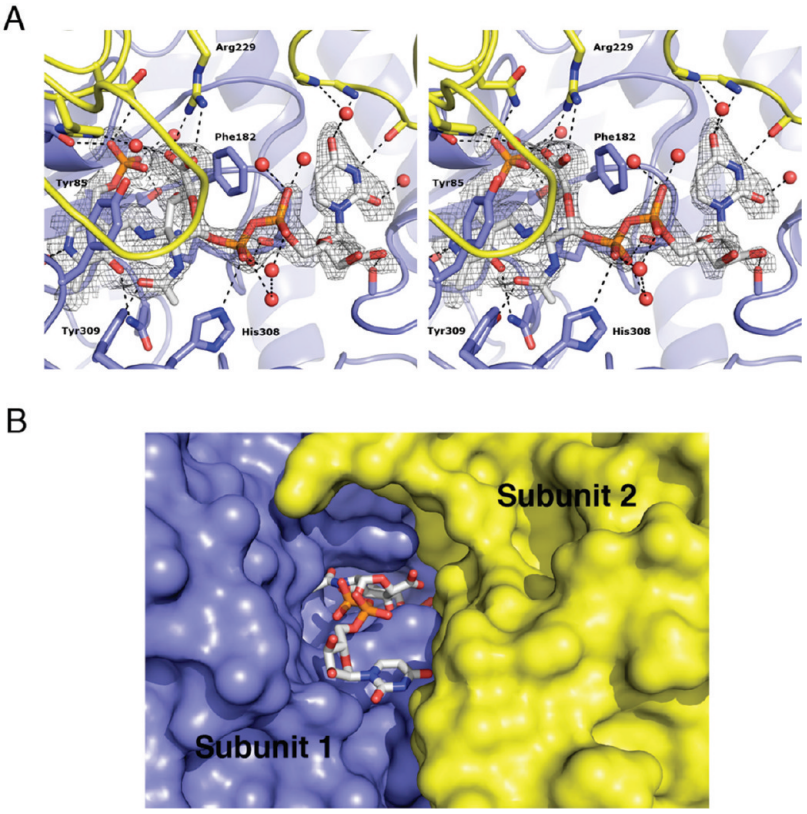

FIGURE 5: Close-up view of the external aldimine-bound structure. (A) External aldimine of PLP and UDP-GlcNAc(3NH$_2$)A in the active site of WbpE. The $2(F_o - F_c)$ electron density map is contoured at 1.5σ and was calculated with atoms of the external aldimine omitted. Residues within a 4 Å radius of the ligand are indicated, and water molecules are depicted as red spheres. (B) Space-filling model of the WbpE external aldimine complex, highlighting the manner in which the uridine moiety extends up through the deep cavity to the solvent. In both figures, the subunits of the dimer are colored blue and yellow.

The glucopyranose ring of the ligand is bound to the cofactor through the C3″ carbon atom, and as depicted in Figure 5, many interactions take place between this highly functionalized sugar and the protein to accommodate it within the active site. The aromatic side chains of Tyr85 and Phe182 are stacked above and below the glucopyranose ring, presumably forming a barrier to prevent solvent access throughout the course of catalysis. In addition, these residues may serve to stabilize the positively charged reaction intermediates through cation−π interactions. The C2″ acetamido oxygen participates in hydrogen bonds with both the side chain phenol of Tyr309 and the C5′ hydroxyl group of the cofactor pyridinium ring, while the C4″ hydroxyl is within hydrogen bonding distance of the cofactor phosphoryl group. The C6″ carboxylate is coordinated with a well-ordered water molecule that is hydrogen-bonded to both the phosphate group and the imidazole ring of His213, which is part of the domain-swapped β-hairpin from the neighboring protein subunit. In addition to this water molecule, the carboxylate is held in place by a salt bridge with the guanidinium moiety of Arg229, also from the β-hairpin domain. This arginine residue is commonly found in Fold Type 1 aminotransferases and is believed to play a critical role in binding L-glutamate and α-KG during the course of the reaction (*18*).

The pyrophosphate of the nucleotide sugar extends away from the glucopyranose through the deep protein cavity that leads to the exterior of the protein and is anchored by interactions with Ser184, His308, and at least two well-ordered waters. The uridine emerges from this channel and is fully exposed to the solvent, making van der Waals contacts with one α-helix from each of the dimer subunits and residues from both monomer units on the bottom face and several water molecules from above. The ribose 3′-OH group participates in hydrogen bonds with the N-terminal region of the protein, including the side chain of Glu3 and the backbone carbonyl of Ile5, while the uracil is in the proximity of numerous residues in the neighboring subunit, including Gly29, Tyr31, and Ile32.

Comparison of the WbpE complexes with PMP and the external aldimine reveals that as in the case with the internal aldimine structure, no major conformational change is observed in the overall architecture of the protein upon substrate binding. Analysis of the overlaid cofactor and external aldimine-bound structures indicates only small differences between the two forms of the enzyme (rmsd = 0.33 Å), with the most notable changes within the domain-swapped β-hairpin shifting slightly around the enzyme active site.

Analysis of WbpE Alanine Mutants. Comparison of the cofactor- and nucleotide sugar-bound structures of WbpE led to the identification of eight key amino acid residues that appear to play a critical role in substrate binding. These residues are found in both subunits of the dimer and contact the cofactor and/or substrate through either hydrogen bonding (Thr60, Gln159, Ser180, Asn227, His308, and Tyr309) or a salt bridge (Asp156 and Arg229). The conservation of many of these residues in the binding sites of other nucleotide sugar aminotransferases also suggests that they may be crucial for enzyme function (*20*, *24*). To explore whether these residues were indeed critical for catalysis, a panel of nine WbpE alanine mutants was generated using site-directed mutagenesis. In addition to eight residues identified above, a mutant in which the catalytic lysine (Lys185) was replaced with alanine was prepared as well. All mutants were

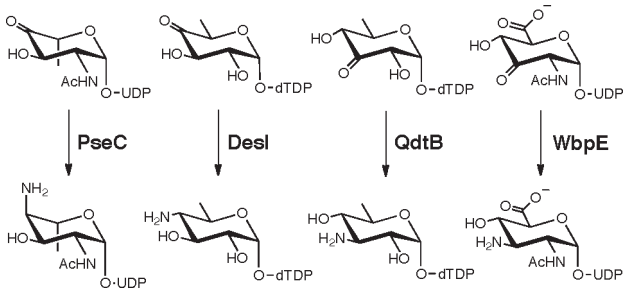

FIGURE 6: Reactions conducted by homologous nucleotide sugar aminotransferases PseC, DesI, QdtB, and WbpE. All reactions require PLP and the concomitant conversion of L-glutamate to α-ketoglutarate.

purified as outlined above to high yield and then tested for activity using the WbpB/WbpE coupled enzyme assay as previously described (*15*) (Figure S2 of the Supporting Information). As anticipated, the activity of the Lys185Ala mutant was completely abolished, but the other eight mutants exhibited nearly complete turnover of substrate to product under these reaction conditions, suggesting that the loss of binding affinity of any one of these residues may be offset by the cumulative efforts of the others. Individual reaction rates were not determined because of the difficulty in isolating the extremely labile ketone substrate of WbpE as well as the need for using the coupled WbpB/WbpE assay, which would mask the effect of a point mutation on the aminotransferase alone.

DISCUSSION

The glycosylation of proteins and lipids is a key post-translational modification common to all three kingdoms of life. These glycans serve to modulate the protein and lipid function in a vast number of ways, affecting processes such as cellular signaling, protein folding, and the immune response. Despite the myriad cellular functions associated with these carbohydrates, the biosynthesis of monosaccharides in all organisms shares several common features, one being their activation as nucleotide sugars. In recent years, there has been a concerted effort to understand the biosynthetic machinery required for the elaboration of these conserved building blocks, particularly in bacteria, where they are found as part of natural products as well as components of the complex cell wall structures. To that end, we present the crystal structure of the UDP-GlcNAc(3keto)A aminotransferase WbpE from *P. aeruginosa* in complex with PMP, PLP, and the external aldimine of PLP with its aminated product. This study represents the first structure of an aminotransferase that binds a nucleotide sugar modified at the C2″, C3″, and C6″ positions. To date, there are three other known structures of Fold Type 1 aminotransferases bound to their nucleotide sugar substrates as the external aldimine (Figure 6). The first complex reported was that of PseC, an aminotransferase from *Helicobacter pylori* involved in the biosynthesis of pseudaminic acid (*20*). Shortly thereafter, the structures of both DesI, a key enzyme in the *Streptomyces venezuelae* desosamine biosynthesis pathway, and QdtB, an aminotransferase required for synthesis of dTDP-Qui*p*3NAc, were presented (*22*, *24*). Taken together, these structures provide an opportunity to gain a deeper understanding of the substrate specificity that governs the function of these enzymes.

A comparison of the active site orientations of the external aldimines in the four known structures (WbpE, PseC, DesI, and QdtB) is presented in Figure 7. It can be seen that while the ligands are positioned quite differently within the binding sites depending primarily on the functional groups on the hexose rings, the structures do share some common features. As expected, the PLP cofactors are positioned in the same basic orientation. Also, each of the four hexose substrates contains a hydroxyl group at either the C3″ (QdtB and WbpE) or C4″ (PseC and DesI) position, and these hydroxyls are all situated on the same side of the active site near the catalytic lysine and the cofactor phosphate or an asparagine, in the case of DesI. Interestingly, all four hexoses seem to be bordered on the top and bottom faces by aromatic side chains, effectively sealing them off from the surrounding environment. One explanation for this observation is that association with these aromatic rings may serve to both stabilize the positively charged reaction intermediates through cation−π interactions and also prevent unwanted water molecules from entering into the active site and interfering with catalysis.

The many differences in nucleotide sugar orientation within the active site depicted in this analysis provide a glimpse into the requirements for substrate binding and specificity. In general, the hexose rings with smaller functional groups and less polarity are in contact with fewer atoms within the active site. This is rather unexpected, as often substrate binding causes conformational changes within the enzyme active site to create an induced fit. For example, while the nucleotide sugars bound to QdtB and WbpE are both anchored to the cofactor through the C3″ position, the QdtB ligand makes far fewer contacts to the active site atoms because of the smaller hexose modifications than the highly functionalized WbpE ligand. Similarly, the C6″ hexose carbons of the QdtB, PseC, and WbpE ligands are all pointing in the same general direction, yet while there are no atoms within 4 Å of the QdtB and PseC C6″ methyl groups, the C6″ carboxylate of WbpE is coordinated to both Arg229 in the β-hairpin domain and to a well-ordered water molecule. It is tempting to propose a relationship between increased space around the ligand hexose ring and decreased enzyme specificity. In their study of QdtB, Thoden et al. made a preliminary effort to address this theory by showing that QdtB accepts the C4″ epimer of its natural substrate, presumably due to the lack of protein contacts between the C4″ position of the hexose and the active site (*24*). However, further biochemical and biophysical studies are required to explore this hypothesis.

The WbpE structure in complex with its external aldimine intermediate described in this report provides the first example of a nucleotide sugar modified at the C6″ position within the enzyme active site. As mentioned previously, the C6″ carboxylate of the ligand is coordinated to Arg229 in the domain-swapped β-hairpin. This arginine residue is commonly found in Fold Type I aminotransferases and has been shown to coordinate with the carboxylate of L-glutamate and α-KG in the first half of the reaction mechanism (*18*). Although there is as yet no direct evidence for where these two molecules bind within the WbpE active site, the crystal structure of a related aminotransferase, ArnB, was recently determined in a complex with α-KG and clearly implicates this arginine in α-KG binding (*19*). Presuming that α-KG is present in the same location in WbpE as it is in ArnB, we can then infer that Arg229 of WbpE interacts with both enzyme substrates (L-glutamate and UDP-GlcNAc(3keto)A), playing a critical role in both halves of the catalytic cycle. This alignment of α-KG and the UDP-GlcNAc(3keto)A substrates within the active site of WbpE complements previous work in our laboratory on this pathway, in which we postulated that the

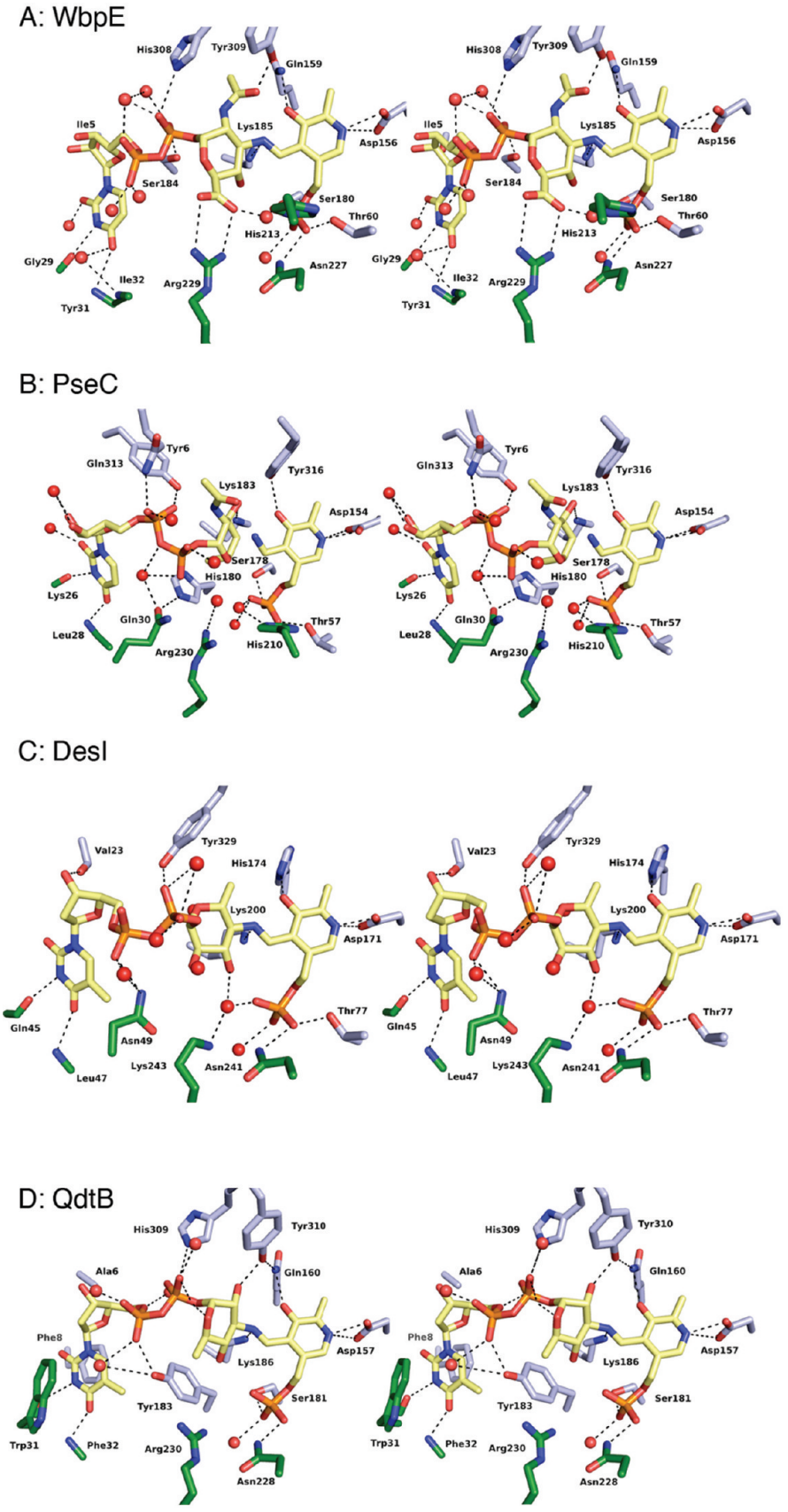

FIGURE 7: Comparison of the structures of WbpE (A), PseC (B), DesI (C), and QdtB (D) in complex with the corresponding external aldimines. For each structure, subunit 1 is colored gray and residues from the domain-swapped hairpin of the neighboring subunit are colored green. Interactions within 3.6 Å of the ligand are shown as black lines, and residues lining the top face of the enzyme were removed for the sake of clarity. All four complexes are positioned with the PLP cofactor in the same orientation to highlight the differences in ligand conformation in each active site. In addition, the basic residue in each enzyme important for α-KG binding (Arg or Lys) is specifically labeled.

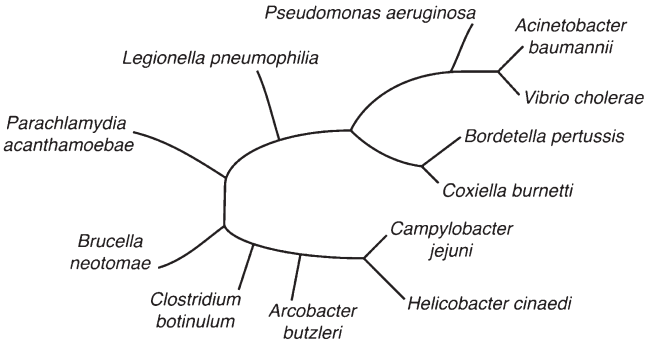

FIGURE 8: Phylogenetic tree indicating homologues of WbpE from pathogenic bacteria. Each homologue indicated has a sequence identity with respect to WbpE of >40%. A full sequence alignment is depicted in Figure S4 of the Supporting Information.

unique NAD^+ cofactor regeneration exhibited by the dehydrogenase WbpB was facilitated by the overlap of α-KG and UDP-GlcNAc(3keto)A within the substrate-binding pocket (*15*).

Another interesting feature of the WbpE structure is the presence of a non-prolyl *cis* amide bond between residues His308 and Tyr309 (Figure S3 of the Supporting Information). The side chains of both of these residues line the active site of the protein and participate in important contacts with the nucleotide sugar to orient it properly. Studies of the prevalence of non-prolyl *cis* amide bonds within protein structures deposited in the Protein Data Bank indicate that they are extremely rare because of the increased steric strain between the neighboring Cα atoms. Interestingly, these *cis* bonds are often found within functionally important regions of the protein. In addition, more than one-third of the characterized proteins containing *cis* amide bonds are present in carbohydrate-binding proteins (*43*). As depicted in Figures 5 and 7, both His308 and Tyr309 participate in key hydrogen bonds with the external aldimine intermediate, framing the upper region of the active site. However, it is clear that these residues are not absolutely crucial for catalysis, as our studies using alanine mutations at these positions still yielded a functional enzyme (Figure S2 of the Supporting Information). The proximity of both His308 and Tyr309 to the hexose and pyrophosphate moieties held in place by the *cis* amide bond suggests that perhaps these residues impart specificity to the enzyme, effectively allowing only substrates of a certain shape to fit in the active site. Further biochemical analysis is required to explore this hypothesis, but difficulty in obtaining the ketone substrate of WbpE complicates these efforts.

While eukaryotes utilize only a limited set of carbohydrates as the basic building blocks for protein glycosylation, prokaryotes routinely incorporate a far greater number of sugar structures to maintain the sheer complexity and diversity of their glycans (*44*). Biochemical evidence has suggested that despite this structural diversity, diacetylated aminuronic acids such as ManNAc(3NAc)A are exceedingly rare. This class of highly functionalized sugars has primarily been identified in the complex cell wall matrices of a few pathogenic bacteria, such as *P. aeruginosa* and *Bordetella pertussis*, as well as the flagellar glycoproteins of certain methanogenic archaea (*45*, *46*). However, an analysis of the rapidly growing database of newly sequenced prokaryotic genomes suggests that perhaps these aminuronic acids are more prevalent than previously suspected. A recent search for WbpE homologues resulted in more than 50 matches with a high degree of sequence identity (>40%); the 11 closest homologues are presented in Figure 8, and a full sequence alignment is provided in Figure S4 of the Supporting Information. Interestingly, these homologues are all found in pathogenic bacteria, many of which have not been subject to in-depth biochemical characterization. The presence of WbpE homologues in these organisms may imply that a ManNAc(3NAc)A-type carbohydrate exists in the cell wall matrix, where it could play a contributing role in modulating virulence and evasion of host defenses, though more work is required to characterize the cell wall components of these organisms to confirm their chemical makeup. Nevertheless, the protein structures reported in this study may offer insight into the biosynthetic enzymes in other pathogenic organisms and provide a unique opportunity for identification of important new targets for antibacterial drug development.

ACKNOWLEDGMENT

We are grateful to the staff at beamline X6A at the National Synchrotron Light Source, particularly Dr. Jean Jakoncic for assistance with data collection and analysis. Special thanks to Debby Pheasant of the Biophysical Instrumentation Facility at the Massachusetts Institute of Technology (MIT) for assistance with analytical centrifugation, Dr. Robert Grant of the Biology Department and members of the Drennan laboratory at MIT for technical advice, and colleagues in the Imperiali laboratory, especially Dr. Matthieu Sainlos, Dr. Jerry Troutman, and Meredith Hartley, for insight and helpful discussions.

SUPPORTING INFORMATION AVAILABLE

Sedimentation velocity analytical ultracentrifugation data, analysis of WbpE alanine mutants and the His308−Tyr309 *cis* amide bond, and a sequence alignment of WbpE homologues from pathogenic bacteria. This material is available free of charge via the Internet at http://pubs.acs.org.

REFERENCES

1. Pier, G. B. (2007) *Pseudomonas aeruginosa* lipopolysaccharide: A major virulence factor, initiator of inflammation and target for effective immunity. *Int. J. Med. Microbiol. 297*, 277–295.
2. Obritsch, M. D., Fish, D. N., MacLaren, R., and Rose, J. (2005) Nosocomial infections due to multidrug-resistant *Pseudomonas aeruginosa*: Epidemiology and treatment options. *Pharmacotherapy 25*, 1353–1364.
3. Tang, H. B., DiMango, E., Bryan, R., Gambello, M., Iglewski, B. H., Goldberg, J. B., and Prince, A. (1996) Contribution of specific *Pseudomonas aeruginosa* virulence factors to pathogenesis of pneumonia in a neonatal mouse model of infection. *Infect. Immun. 64*, 37–43.
4. Diaz, M. H., Shaver, C. M., King, J. D., Musunuri, S., Kazzaz, J. A., and Hauser, A. R. (2008) *Pseudomonas aeruginosa* induces localized immunosuppression during pneumonia. *Infect. Immun. 76*, 4414–4421.
5. Son, M. S., Matthews, W. J., Jr., Kang, Y., Nguyen, D. T., and Hoang, T. T. (2007) In vivo evidence of *Pseudomonas aeruginosa* nutrient acquisition and pathogenesis in the lungs of cystic fibrosis patients. *Infect. Immun. 75*, 5313–5324.
6. Levy, S. B., and Marshall, B. (2004) Antibacterial resistance worldwide: Causes, challenges and responses. *Nat. Med. 10*, S122–S129.
7. Mesaros, N., Nordmann, P., Plesiat, P., Roussel-Delvallez, M., Van Eldere, J., Glupczynski, Y., Van Laethem, Y., Jacobs, F., Lebecque, P., Malfroot, A., Tulkens, P. M., and Van Bambeke, F. (2007) *Pseudomonas aeruginosa*: Resistance and therapeutic options at the turn of the new millennium. *Clin. Microbiol. Infect. 13*, 560–578.
8. Hancock, R. E. (1998) Resistance mechanisms in *Pseudomonas aeruginosa* and other nonfermative gram-negative bacteria. *Clin. Infect. Dis. 27*, S93–S99.
9. Cryz, S. J., Jr., Pitt, T. L., Furer, E., and Germanier, R. (1984) Role of lipopolysaccharide in virulence of *Pseudomonas aeruginosa*. *Infect. Immun. 44*, 508–513.
10. Hancock, R. E., Mutharia, L. M., Chan, L., Darveau, R. P., Speert, D. P., and Pier, G. B. (1983) *Pseudomonas aeruginosa* isolates from

patients with cystic fibrosis: A class of serum-sensitive, nontypable strains deficient in lipopolysaccharide O side chains. *Infect. Immun. 42*, 170–177.
11. Engels, W., Endert, J., Kamps, M. A., and van Boven, C. P. (1985) Role of lipopolysaccharide in opsonization and phagocytosis of *Pseudomonas aeruginosa*. *Infect. Immun. 49*, 182–189.
12. Dasgupta, T., de Kievit, T. R., Masoud, H., Altman, E., Richards, J. C., Sadovskaya, I., Speert, D. P., and Lam, J. S. (1994) Characterization of lipopolysaccharide-deficient mutants of *Pseudomonas aeruginosa* derived from serotypes O3, O5, and O6. *Infect. Immun. 62*, 809–817.
13. Kochetkov, N. K., and Knirel, Y. A. (1994) Structure of lipopolysaccharides from gram-negative bacteria. III. Structure of O-specific polysaccharides. *Biochemistry* (*Moscow, Russ. Fed.*) *59*, 1325–1383.
14. Rocchetta, H. L., Burrows, L. L., and Lam, J. S. (1999) Genetics of O-antigen biosynthesis in *Pseudomonas aeruginosa*. *Microbiol. Mol. Biol. Rev. 63*, 523–553.
15. Larkin, A., and Imperiali, B. (2009) Biosynthesis of UDP-GlcNAc-(3NAc)A by WbpB, WbpE, and WbpD: Enzymes in the Wbp Pathway Responsible for O-Antigen Assembly in *Pseudomonas aeruginosa* PAO1. *Biochemistry 48*, 5446–5455.
16. Burrows, L. L., Charter, D. F., and Lam, J. S. (1996) Molecular characterization of the *Pseudomonas aeruginosa* serotype O5 (PAO1) B-band lipopolysaccharide gene cluster. *Mol. Microbiol. 22*, 481–495.
17. John, R. A. (1995) Pyridoxal phosphare-dependent enzymes. *Biochim. Biophys. Acta 1248*, 81–96.
18. Eliot, A. C., and Kirsch, J. F. (2004) Pyridoxal Phosphate Enzymes: Mechanistic, Structural, and Evolutionary Considerations. *Annu. Rev. Biochem. 73*, 383–415.
19. Noland, B. W., Newman, J. M., Hendle, J., Badger, J., Christopher, J. A., Tresser, J., Rutter, M. E., Sanderson, W. E., Müller-Dieckmann, H.-J., Gajiwala, K. S., and Buchanan, S. G. (2002) Structural Studies of *Salmonella typhimurium* ArnB (PmrH) Aminotransferase: A 4-Amino-4-deoxy-L-arabinose Lipopolysaccharide-Modifying Enzyme. *Structure* (*Cambridge, MA, U.S.*) *10*, 1569–1580.
20. Schoenhofen, I. C., Lunin, V. V., Julien, J.-P., Li, Y., Ajamian, E., Matte, A., Cygler, M., Brisson, J.-R., Aubry, A., Logan, S. M., Bhatia, S., Wakarchuk, W. W., and Young, N. M. (2006) Structural and Functional Characterization of PseC, an Aminotransferase Involved in the Biosynthesis of Pseudaminic Acid, an Essential Flagellar Modification in *Helicobacter pylori*. *J. Biol. Chem. 281*, 8907–8916.
21. Burgie, E. S., Thoden, J. B., and Holden, H. M. (2007) Molecular architecture of DesV from *Streptomyces venezuela*e: A PLP-dependent transaminase involved in the biosynthesis of the unusual sugar desosamine. *Protein Sci. 16*, 887–896.
22. Burgie, E. S., and Holden, H. M. (2007) Molecular Architecture of DesI: A Key Enzyme in the Biosynthesis of Desosamine. *Biochemistry 46*, 8999–9006.
23. Cook, P. D., and Holden, H. M. (2008) GDP-Perosamine Synthase: Structural Analysis and Production of a Novel Trideoxysugar. *Biochemistry 47*, 2833–2840.
24. Thoden, J. B., Schäffer, C., Messner, P., and Holden, H. M. (2009) Structural Analysis of QdtB, an Aminotransferase Required for the Biosynthesis of dTDP-3-acetamido-3,6-dideoxy-α-D-glucose. *Biochemistry 48*, 1553–1561.
25. Van Duyne, G. D., Standaert, R. F., Karplus, P. A., Schreiber, S. L., and Clardy, J. (1993) Atomic Structures of the Human Immunophilin FKBP-12 Complexes with FK506 and Rapamycin. *J. Mol. Biol. 29*, 105–124.
26. Stafford, W. F., and Sherwood, P. J. (2004) Analysis of heterologous interacting systems by sedimentation velocity: Curve fitting algorithms for estimation of sedimentation coefficients, equilibrium and kinetic constants. *Biophys. Chem. 108*, 231–243.
27. Otwinowski, Z., and Minor, W. (1997) Processing of X-ray Diffraction Data Collected in Oscillation Mode. *Methods Enzymol. 276*, 307–326.
28. Collaborative Computational Project Number 4 (1994) The CCP4 Suite: Programs for Protein Crystallography. *Acta Crystallogr. D50*, 760–763.
29. Hendrickson, W. A. (1991) Determination of macromolecular structures from anomalous diffraction of synchrotron radiation. *Science 254*, 51–58.
30. Terwilliger, T. C., and Berendzen, J. (1999) Automated MAD and MIR structure solution. *Acta Crystallogr. D55*, 849–861.
31. Terwilliger, T. C. (2003) Automated main-chain model building by template matching and iterative fragment extension. *Acta Crystallogr. D59*, 38–44.
32. Terwilliger, T. C. (2000) Maximum-likelihood density modification. *Acta Crystallogr. D56*, 965–972.
33. Storoni, L. C., McCoy, A. J., and Read, R. J. (2004) Likelihood-enhanced fast rotation functions. *Acta Crystallogr. D60*, 432–438.
34. Emsley, P., and Cowtan, K. (2004) Coot: Model-building tools for molecular graphics. *Acta Crystallogr. D60*, 2126–2132.
35. Murshudov, G. N., Vagin, A. A., and Dodson, E. J. (1997) Refinement of Macromolecular Structures by the Maximum-Likelihood Method. *Acta Crystallogr. D53*, 240–255.
36. Brünger, A. T. (1993) Assessment of Phase Accuracy by Cross Validation: The Free *R* Value, Methods and Applications. *Acta Crystallogr. D49*, 24–36.
37. Lamzin, V. S., Perrakis, A., and Wilson, K. S. (2001) The ARP/wARP suite for automated construction and refinement of protein models. In International Tables for Crystallography (Rossmann, M. G., and Arnold, E., Eds.) pp 720−722, Kluwer Academic Publishers, Dordrecht, The Netherlands.
38. Laskowski, R. A., MacArthur, M. W., Moss, D. S., and Thornton, J. M. (1993) PROCHECK: A program to check the stereochemical quality of protein structures. *J. Appl. Crystallogr. 26*, 283–291.
39. Vaguine, A. A., Richelle, J., and Wodak, S. J. (1998) SFCHECK: A unified set of procedures for evaluating the quality of macromolecular structure-factor data and their agreement with the atomic model. *Acta Crystallogr. D55*, 191–205.
40. Davis, I. W., Leaver-Fay, A., Chen, V. B., Block, J. N., Kapral, G. J., Wang, G. J., Wang, X., Murray, L. W., Arendal, B., III, Snoeyink, J., Richardson, J. S., and Richardson, D. C. (2007) MolProbity: All-atom contacts and structure validation for proteins and nucleic acids. *Nucleic Acids Res. 35*, W375–W383.
41. Ford, G. C., Eichele, G., and Jansonius, J. N. (1980) Three-dimensional structure of a pyridoxal-phosphate-dependent enzyme, mitochondrial aspartate aminotransferase. *Proc. Natl. Acad. Sci. U.S.A. 77*, 1559–2563.
42. Jansonius, J. N. (1998) Structure, evolution and action of vitamin B_6-dependent enzymes. *Curr. Opin. Struct. Biol. 8*, 759–769.
43. Jabs, A., Weiss, M. S., and Hilgenfeld, R. (1999) Non-proline cis peptide bonds in proteins. *J. Mol. Biol. 286*, 291–304.
44. Varki, A., Cummings, R. D., Freeze, H. H., Stanley, P., Bertozzi, C. R., Hart, G. W., and Etzler, M. E. (2008) Essentials of Glycobiology, 2nd ed., Cold Spring Harbor Laboratory Press, Plainview, NY.
45. Kelly, J., Logan, S. M., Jarrell, K. F., VanDyke, D. J., and Vinogradov, E. V. (2009) A novel *N*-linked flagellar glycan from *Methanococcus maripalidus*. *Carbohydr. Res. 344*, 648–653.
46. Caroff, M., Brisson, J.-R., Martin, A., and Karibian, D. (2000) Structure of the *Bordetella pertussis* 1414 endotoxin. *FEBS Lett. 477*, 8–14.